Am J Cancer Res 2026;16(5):2040-2054
www.ajcr.us /ISSN:2156-6976/ajcr0170485

Original Article

Schisandrin A suppresses hepatocellular carcinoma and sensitizes to sorafenib via modulating retinol metabolism

Yu Zhou[1,2,5*], Yufan Mao[1*], Xueliang Fu[1], Yanan Li[2,4], Meng Xu[6], Deliang Zhou[3], Shuai Zha[1,2]

[1]School of Laboratory Medicine, Hubei University of Chinese Medicine, No. 16 Huangjiahu West Road, Hongshan District, Wuhan 430065, Hubei, PR China; [2]Hubei Shizhen Laboratory, No. 4 Huayuanshan, Wuchang District, Wuhan 430060, Hubei, PR China; [3]Department of General Surgery, Affiliated Hospital of Hubei University of Chinese Medicine, Hubei Provincial Hospital of Traditional Chinese Medicine, Hubei Province Academy of Traditional Chinese Medicine, No. 4 Huayuanshan, Wuchang District, Wuhan 430060, Hubei, PR China; [4]School of Acupuncture-Moxibustion and Orthopedics, Hubei University of Chinese Medicine, No. 188 Tanhualin, Wuchang District, Wuhan 430060, Hubei, PR China; [5]Research and Development Center of Science and Technology, Wuhan University, No. 299 Bayi Road, Wuchang District, Wuhan 430072, Hubei, PR China; [6]Department of Traditional Chinese Medicine, Maternal and Child Health Hospital of Hubei Province, No. 745 Wuluo Road, Hongshan District, Wuhan 430070, Hubei, PR China. [*]Co-first authors.

Received December 3, 2025; Accepted May 19, 2026; Epub May 25, 2026; Published May 30, 2026

Abstract: Hepatocellular carcinoma (HCC) is usually diagnosed at an advanced stage, where first-line sorafenib therapy frequently encounters acquired resistance. Natural compounds derived from traditional medicine may provide alternative strategies to address this challenge. Here, we show that Schisandrin A, a lignan from *Schisandra Chinensis*, inhibits HCC cell proliferation and induces G1/S cell cycle arrest *in vitro* while also downregulating sorafenib-resistance genes and increasing sorafenib sensitivity. In a xenograft model, Schisandrin A acted synergistically with sorafenib to improve antitumor efficacy without increasing toxicity. Supported by multi-omics analyses indicating the involvement of retinol metabolism regulation. These findings identify Schisandrin A as a potential adjunctive agent for overcoming sorafenib resistance in advanced HCC.

Keywords: Hepatocellular carcinoma, Schisandrin A, sorafenib, cell cycle arrest, retinol metabolism

Introduction

Hepatocellular carcinoma (HCC) is still the most common type of primary liver cancer. HCC incidence and mortality both continue to increase all over the world. Being an early-stage disease is usually asymptomatic, early detection is very challenging in clinical practice. As such, most HCC patients are found at advanced stages at which curative surgery is no longer an option. Thus, non-surgical treatments including systemic therapies stand out as treatment options for advanced HCC patients [1]. Introduction of sorafenib as the first approved targeted treatment for HCC was a major breakthrough of first-line treatment. However, the real clinical benefit of sorafenib is limited. Although sorafenib therapy can prolong median overall survival in patients with advanced HCC, the benefit is only about 3 months, with a very low objective response rate. Of note, acquired drug resistance usually develops after 4 to 5 months of therapy, thus severely eroding its long-term efficacy of this agent [2, 3]. Despite such limitations, there is great need to search for new agents able to sensitize malignant lesions to available targeted treatments or to enhance the effects of available targeted agents. Progress in this field will be critical to improving outcomes in patients with HCC.

Derived mainly from nature, TCM is a promising source for modern drug discovery. Various studies have shown that TCM compounds and traditional Chinese herbal medicines exhibit much lower toxicity than that of normal chemotherapeutic drugs and thus low adverse reactions in patients [4, 5]. In clinical cancer therapy, the

https://doi.org/10.62347/SPOL6693

use of TCM has shown great therapeutic efficacy. The incorporation of some TCM formulas into the traditional treatment plan can mitigate significantly the adverse effects of chemical chemotherapy. This strategy is paired with improved patient survival and a better quality of life [6, 7]. Moreover, the concurrent use of TCM agents together with the conventional cancer drugs increases the overall efficacy of cancer therapy, which is obviously attributable to their underlying synergistic or sensitizing effects [8].

Extracted from the dried ripe fruit of *Schisandra chinensis*, the lignan component Schisandrin A (deoxyschizandrin) is a major effective component of a traditional Chinese herb [9, 10]. Many reported works demonstrate diverse biological activities of Schisandrin A in various disease models, such as antioxidant [11-13] and anti-inflammatory [14, 15] properties, for example. Notably, the clinical contribution of Schisandrin A in the field of cancer therapy are also emerging. Schisandrin A has been reported to inhibit the development of some cancers, such as the non-small cell lung cancer (NSCLC) [16, 17], prostate cancer [18], colorectal cancer [19], and bladder cancer [20]. However, whether Schisandrin A can exert antitumor effects on HCC and how it plays such effects have remained largely unclear.

Addressing this knowledge gap, in the present study, we explored the specific impact of Schisandrin A on HCC. We showed that this compound significantly inhibits the proliferation of HCC cells and induce cell cycle arrest of HCC cells *in vitro*. Moreover, transcriptome sequencing found that Schisandrin A sensitizes HCC cells to sorafenib, the typical first-line targeted drug for treating advanced HCC. This sensitizing effect was verified *in vivo* in a mouse xenograft model; Schisandrin A administration could significantly enhance the antitumor effect of sorafenib. Overall, our study elucidated the mechanism of action of Schisandrin A antitumor effect on HCC and highlighted its ability as a tumor sensitizer, therefore giving experimental evidence for its potential clinical usage in the future.

Methods and materials

Cell cycle analysis

Cell cycle distribution was analyzed by PI staining using a cell cycle detection kit (Beyotime, C1062S) according to the manufacturer's instruction (Beyotime, C1052). Briefly, L02, Huh7, MHCC97H cells were seeded in 6-well plates at a density of 2×10^5 cells per well and treated with Schiszandrin A (TOPSCIENCE, T2926) at different concentrations for 24 h. Following treatment, both adherent and floating cells were collected and combined. Then, cells were fixed in 70% ethanol were treated with RNase A and PI (50 μg/mL). DNA content was measured using a flow cytometer (CytoFLEX, BECKMAN). Data were processed with FlowJo software (version 10.8).

Cell apoptosis analysis

Cell apoptosis was quantitatively assessed using an Annexin V-FITC/PI apoptosis detection kit (Beyotime, C1062S). Briefly, L02, Huh7, and MHCC97H cells were seeded in 6-well plates at a density of 2×10^5 cells per well and treated with various concentrations of Schisandrin A for 24 h. After treatment, both adherent and floating cells were collected, washed with cold PBS, and resuspended in binding buffer. A 100 μL aliquot of cell suspension was stained with 5 μL Annexin V-FITC and 5 μL PI, followed by 15 min incubation in the dark. Subsequently, 400 μL of binding buffer was added, and samples were immediately analyzed on a CytoFLEX flow cytometer (BECKMAN), acquiring at least 10,000 events per sample. Cell populations were distinguished as viable (Annexin V^-/PI^-), early apoptotic (Annexin V^+/PI^-), late apoptotic/necrotic (Annexin V^+/PI^+), and necrotic (Annexin V^-/PI^+) using FlowJo software (v10.8). All experiments were independently repeated three times.

CCK-8 assay and synergistic inhibition analysis

Cell viability was assessed by a Cell Counting Kit-8 (CCK-8, TOPSCIENCE, C0005). Briefly, the L02, Huh7, MHCC97H cells were seeded in 96-well plates at the density of 20,000 cells per well. After adherence for 24 h, the cells were treated with various concentrations of Schisandrin/Sorafenib (MedChemExpress, HY-10201) for 24 h. Subsequently, 10 μL CCK-8 reagent was added into each well and the plate incubated for 3 h at 37°C. The absorbance was measured at 450 nm with a microplate reader. Cell viability was calculated based on the untreated control group and the half maximal inhibitory concentration (IC_{50}) of drugs was calcu-

lated from dose response curves with nonlinear regression. Synergistic inhibitory effects of SchA and Sorafenib were plotted by SynergyFinder (https://synergyfinder.org/).

Colony formation assay

To examine the long-term clonogenic survival of L02, Huh7, MHCC97H cells with the treatment of Schisandrin A, colony formation assay was conducted. Briefly, the cells were seeded at low density (2000 cells per well) in a 6-well plate and allowed to adhesion overnight. After an overnight adhesion, the culture medium was replaced with new medium containing the aimed concentration of Schisandrin A for 48 h. The medium containing Schisandrin A was aspirated and gently washed the cells with PBS, and then added into fresh drug-free complete medium, the plate was cultured for another 10 d to promote colonies formation, the medium of plate was replenished every 3 d. After the colony formation, colonies were fixed with 4% paraformaldehyde solution (Servicebio, G1101) and stained with 0.5% crystal violet (Servicebio, G1014) and manually counted; colonies were counted as a cluster of >50 cells. The survival fraction was calculated compared to the control.

Western blot analysis

Western blot analysis was performed to evaluate protein expression levels in response to experimental treatments. Briefly, cells were lysed using RIPA buffer supplemented with protease and phosphatase inhibitors (Beyotime, P1046), and the protein concentration was determined using a BCA assay (Beyotime, P0012). Equal amounts of protein (20-30 μg) were separated by SDS-PAGE and subsequently transferred to PVDF membranes (0.22 μm). The membranes were blocked with 5% non-fat milk in TBST for 1 hour at room temperature and then incubated overnight at 4°C with specific primary antibodies, GAPDH (cell signaling technology, #2118, source: rabbit, 1:5000), β-actin (cell signaling technology, #4967, source: rabbit, 1:5000), p53 (cell signaling technology, #2527, source: rabbit, 1:2000), p-p53 (ser15) (cell signaling technology, #9284, source: rabbit, 1:2000), RB (cell signaling technology, #9309, source: mouse, 1:2000), p-RB (ser780) (cell signaling technology, #8180, source: rabbit, 1:2000). Following extensive washing, the membranes were incubated with HRP-conjugated goat anti rabbit (ABclonal, AS014, 1:5000) or anti mouse (ABclonal, AS003, 1:5000) secondary antibodies for 1 hour at room temperature. Protein bands were visualized using an enhanced chemiluminescence (ECL, BIO-RAD, #1705060) detection system and imaged with a chemiluminescence imaging system (Tanon 4600).

EdU incorporation

The assessment of cell proliferation was performed using a commercial EdU (5-Ethynyl-2'-deoxyuridine) incorporation assay kit (Beyotime, C0071S) according to the manufacturer's instructions. Briefly, cells seeded in 48-well plates were incubated with a 10 μM EdU labeling solution for 4 hours prior to the termination of the experiment. Following the labeling period, cells were fixed with 4% paraformaldehyde (Servicebio, G1101) for 15 minutes and permeabilized with 0.3% Triton X-100 (Servicebio, G1204) for another 15 minutes. The incorporated EdU was then reacted with a fluorescent azide probe via a copper-catalyzed click reaction for 30 minutes in the dark. To visualize all nuclei, cells were counterstained with Hoechst 33342. Fluorescent images were captured using a fluorescence microscope, and the percentage of EdU-positive cells (proliferating cells) relative to the total number of Hoechst-positive cells was automatically quantified using ImageJ software across at least five random fields per well. Each experiment was conducted with a minimum of three replicates and repeated independently three times.

RNA sequencing

Total RNA was isolated from cell samples with TRIzol reagent (Sangon Biotech, #B511311) according to the instruction of the manufacturer, and the library preparation was performed according to the RNA concentration measurement with ultramicrospectrophotometer (Thermo Fisher, NanoDrop 2000). The libraries obtained were sequenced on the DNBSEQ-T7 platform at Beijing Genomics Institute (BGI).

Untargeted metabolomics

Cells were harvested by the digestion of 0.25% trypsin. The supernatant was aspirated and metabolites were extracted by adding the pre-

mixed solvent mixture of methanol, acetonitrile and water (2:2:1, v/v/v), chilled for low-temperature sonication, then samples incubated for protein precipitation at -20°C and, finally, high-speed centrifugation. The collected supernatant was concentrated under vacuum and reconstituted with 100 μl of acetonitrile/water (1:1, v/v). Samples were centrifuged again to get the final supernatant to inject. UHPLC-MS/MS analysis was carried out using an ultra-high performance liquid chromatography system equipped with a HILIC column coupled to a high-resolution mass spectrometer (Orbitrap or Q-TOF). HPLC separation was achieved by gradient elution with water (containing 25 mM of ammonium acetate and 25 mM of ammonia) and acetonitrile as mobile phases. Mass spectra were collected in positive or negative ESI mode to obtain full scan and MS/MS fragmentation spectra. QC samples were evenly inserted during the analysis run for regular monitoring of system conditions. Raw MS data were converted into the format. mzXML with ProteoWizard and imported into XCMS software to analyse peak alignment, retention time calibration and feature peak area extraction. Meanwhile, accurate structural annotation of the metabolites and data normalisation were done by peak area matching of retention time, exact m/z value (mass accuracy error of <10 ppm) and MS/MS spectra with in-house standards of Shanghai Applied Protein Technology database.

Cell-Derived Xenograft (CDX) models

To establish cell-derived xenograft (CDX) model, 5×10^6 Huh7 cells in a 1:1 mixture of matrigel and RPMI-1640 medium were subcutaneously injected into right flank of 6-week-old male BALB/c nude mice. The tumor volume was counted and calculated by the formula: Volume = (Length × Width^2)/2. When the average tumor volume was about 100 mm^3, these tumor-bearing mice were divided randomly into control and treatment groups (n=6 mice in each group). The treatment groups were dosed with Schisandrin A (25 mg/kg), Sorafenib (10 mg/kg) or mixed with each other respectively by gavage of oral administration every day, and the control group was treated with equal amount of saline by oral administration every day. Tumor volume and mouse body weight were measured every 2 days during the period of treatment. Mice were euthanized with carbon dioxide (CO_2) inhalation when the experiment finished, with flow displaced 30%-70% of the amount of the chamber per minute. Then the tumors were excised, weighed and preserved for additional immunohistochemical analysis. All animal experiments were approved by the Animal Care and Use Committee of Hubei University of Chinese Medicine and followed animal welfare regulations (approval no: HUCMS 84481763).

Immunohistochemical staining of Ki67

Immunohistochemical (IHC) staining for Ki67 was conducted on 4-μm-thick, FFPE-tissue sections to determine cell proliferation. Simple. In brief, sections were deparaffinized in xylene and rehydrated by serial concentrations of ethanol. Antigen retrieval was conducted in citrate buffer (pH 6.0) with a microwave heating system. Endogenous peroxidase was quenched with 3% hydrogen peroxide for 15 min. After blocking with 5% normal goat serum for 1 h at room temperature, sections were incubated overnight at 4°C with rabbit polyclonal anti-Ki67 antibody (Abcam, #ab92742) at appropriate optimal dilution (1:500). Sections were then incubated with appropriate HRP-conjugated secondary antibody at room temperature for 1 h and DAB substrate kit (Abcam, #ab64238) was used to develop a signal. Last, sections were counterstained with haematoxylin, dehydrated, cleared and mounted. Twins Ki67 index: The Ki67 proliferation index was calculated as percentage of positive nuclei among the overall number of tumor cells counted in 5 random high power fields.

Bioinformatical analysis

All bioinformatics analyses, including the generation of volcano plots, Venn diagrams, heatmap analysis, LASSO regression, and the performance of Gene Ontology (GO), were conducted employing the Xiantao Academic platform (https://www.xiaotaozi.com). The joint pathway analysis of transcriptomic and metabolomic data was performed using the online analysis tool MetaboAnalyst 6.0 (https://www.metaboanalyst.ca).

Statistical analysis

All statistical analyses were performed using GraphPad Prism (Version 10.0). Data are presented as the mean ± standard deviation (SD),

unless otherwise stated. Differences between two independent groups were assessed using an unpaired Student's *t*-test. For data analysis among multiple groups, a one-way analysis of variance (ANOVA) followed by Tukey's post hoc test was utilized. Comparisons involving multiple time points or repeated measurements were analyzed using a repeated measures ANOVA followed by post hoc test. A two-sided *P* value <0.05 was considered statistically significant.

Results

Schisandrin A suppresses proliferation of hepatocellular carcinoma cells in vitro

To study the anti-tumor effect of schisandrin A (SchA, chemical structure shown in **Figure 1A**) on HCC, we first checked its cytotoxicity against two types of HCC cell lines Huh7 and MHCC97H. As shown in **Figure 1B** and **1C**, SchA showed an IC_{50} value of 43.96 μM and 45.47 μM in Huh7 and MHCC97H cells, respectively, providing reference concentration for the following experiments. EdU incorporation assay showed that SchA dose-dependently reduced the percentage of actively proliferating cells of HCC cells (Supplementary Figure 1). We then checked the long-term proliferative ability of HCC cells by two-dimensional colony formation assay. Treatment with SchA dose-dependently reduced colony formation of Huh7 (**Figure 1D**, **1E**) and MHCC97H (**Figure 1F**, **1G**) cells. To evaluate the tumor-selectivity, we first checked the effect of SchA on non-tumorigenic hepatocyte cell line L02. Interestingly, at the equivalent concentrations, SchA had no effect on the colony forming of L02 (**Figure 1H**, **1I**), which means that SchA has selective cytotoxicity to malignant hepatocytes. In all, these studies showed that SchA impaired the clonogenic ability of HCC cells *in vitro* selectively and did not harm normal hepatocytes.

Schisandrin A arrests HCC cell cycle at G1/S boundary

Subsequently, we further investigated whether the inhibitory effect of SchA on HCC cell proliferation is associated with cell cycle arrest. Cells were stained with propidium iodide (PI), followed by FACS (fluorescence activated cell sorting) analysis of DNA content to determine cell cycle distribution. The results showed that SchA treatment had no significant effect on the cell cycle in L02 cells (**Figure 2A-D**). However, SchA treatment significantly increased the proportion of cells in the G0/G1 phase while decreasing the proportion in the S phase in both Huh7 (**Figure 2E-H**) and MHCC97H (**Figure 2I-L**) cells. These results indicate that SchA induces G1 phase arrest in HCC cells, suggesting it may interfere with the G1/S checkpoint. Therefore, we examined the expression levels of p53 and retinoblastoma protein (RB), which are key regulatory proteins involved in G1/S checkpoint control. p53 is a well-established tumor suppressor, its phosphorylation at ser15 activates downstream signaling pathways, leading to apoptosis or cell cycle arrest, thereby exerting its tumor suppressive function. Western blot analysis revealed that SchA treatment significantly promoted phosphorylation of p53 at Ser15 in both Huh7 (**Figure 2M**, **2N**) and MHCC97H (**Figure 2O**, **2P**) cells. RB is a critical tumor suppressor protein; phosphorylation at ser780 inactivates RB, leading to cell cycle arrest by inhibiting progression through the G1/S checkpoint. Western blot analysis showed that SchA treatment dose-dependently inhibited phosphorylation of RB at ser780 in both Huh7 (**Figure 2Q**, **2R**) and MHCC97H (**Figure 2S**, **2T**) cells. Taken together, these findings demonstrate that Schisandrin A suppresses HCC cell proliferation by inducing G1 phase cell cycle arrest.

Schisandrin A cell exerts no significant effect on apoptosis of HCC cells

Subsequently, we also investigated whether SchA could induce apoptosis in HCC cells. The effect of SchA treatment on apoptosis was analyzed by FACS. The results demonstrated that SchA treatment did not induce significant apoptosis in any of the cell lines tested, including the normal hepatocyte line L02 (**Figure 3A-D**) and the HCC cell lines Huh7 (**Figure 3E-H**) and MHCC97H (**Figure 3I-L**).

Schisandrin A sensitized HCC cells to sorafenib

Sorafenib is a first-line chemotherapeutic agent for HCC in clinical practice. However, its efficacy is often limited by the development of drug resistance in cancer cells. In this study, we investigated whether SchA, an active component derived from traditional Chinese medicine, could reverse sorafenib resistance in HCC cells.

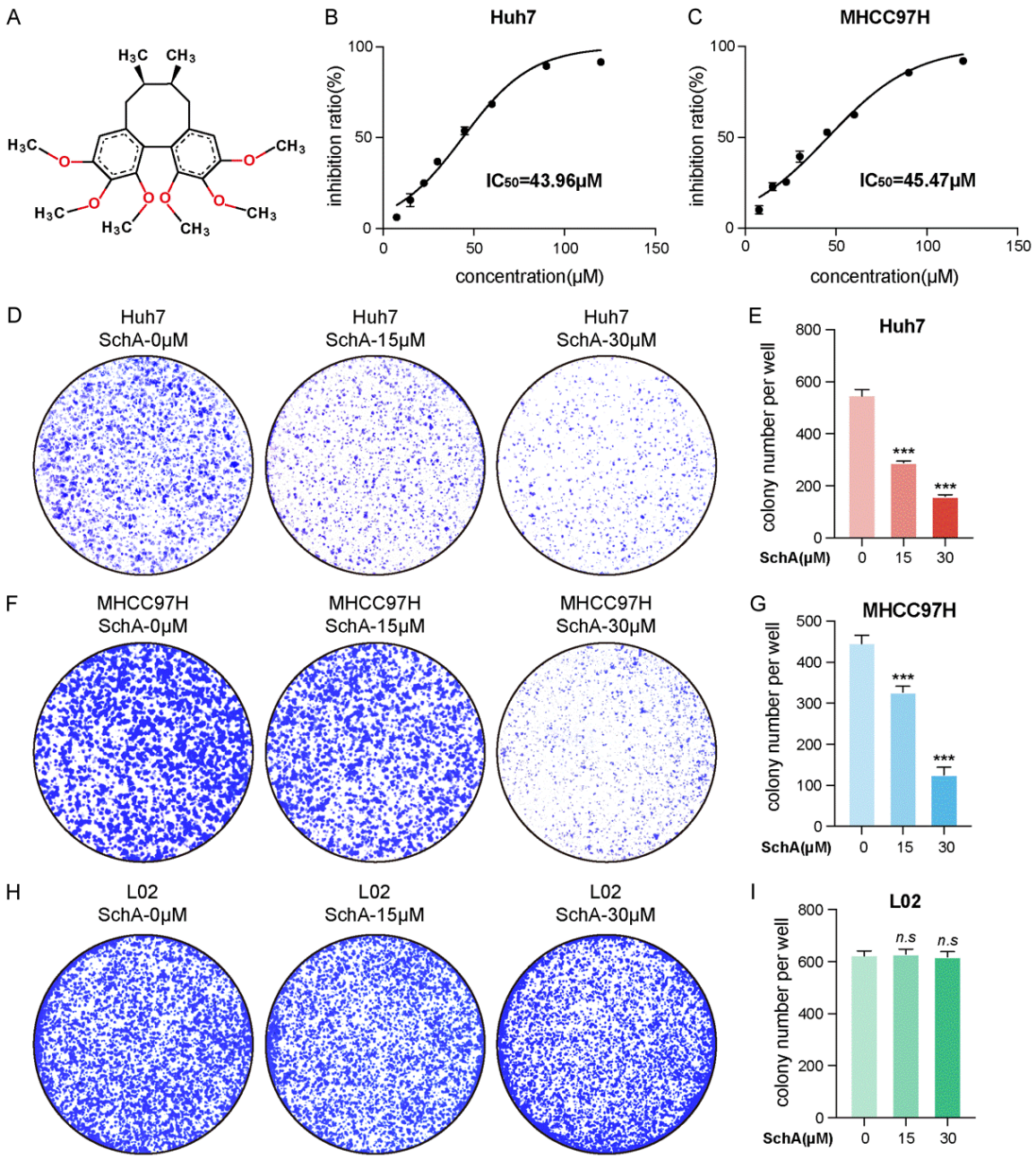

Figure 1. IC_{50} determination of Schisandrin A and colony formation assay in HCC cells. (A) The chemical structure of Schisandrin A. (B) IC_{50} of SchA on Huh7 cells detected by CCK-8. (C) IC_{50} of SchA on MHCC97H cells detected by CCK-8. (D) Representative images of colony formation assay of Huh7 cells treated with different concentration of SchA (0 μM, 15 μM, 30 μM). (E) Statistics of colony number in (D), *n*=3. (F) Representative images of colony formation assay of MHCC97H cells treated with different concentration of SchA (0 μM, 15 μM, 30 μM). (G) Statistics of colony number in (F), *n*=3. (H) Representative images of colony formation assay of L02 cells treated with different concentration of SchA (0 μM, 15 μM, 30 μM). (I) Statistics of colony number in (H), *n*=3. Unpaired Student's *t* test, ***P<0.001, *n.s* represents no significance.

First, we selected two transcriptomic sequencing datasets from the GEO database (GSE242333 and GSE213615), comparing sorafenib-resistant and sorafenib-sensitive Huh7 sublines. We identified differentially expressed genes (DEGs) in the resistant sublines relative to the sensitive ones for each dataset (**Figure 4A**). Subsequently, to identify genes significantly associated with sorafenib resistance in HCC cells, we determined the intersection of the

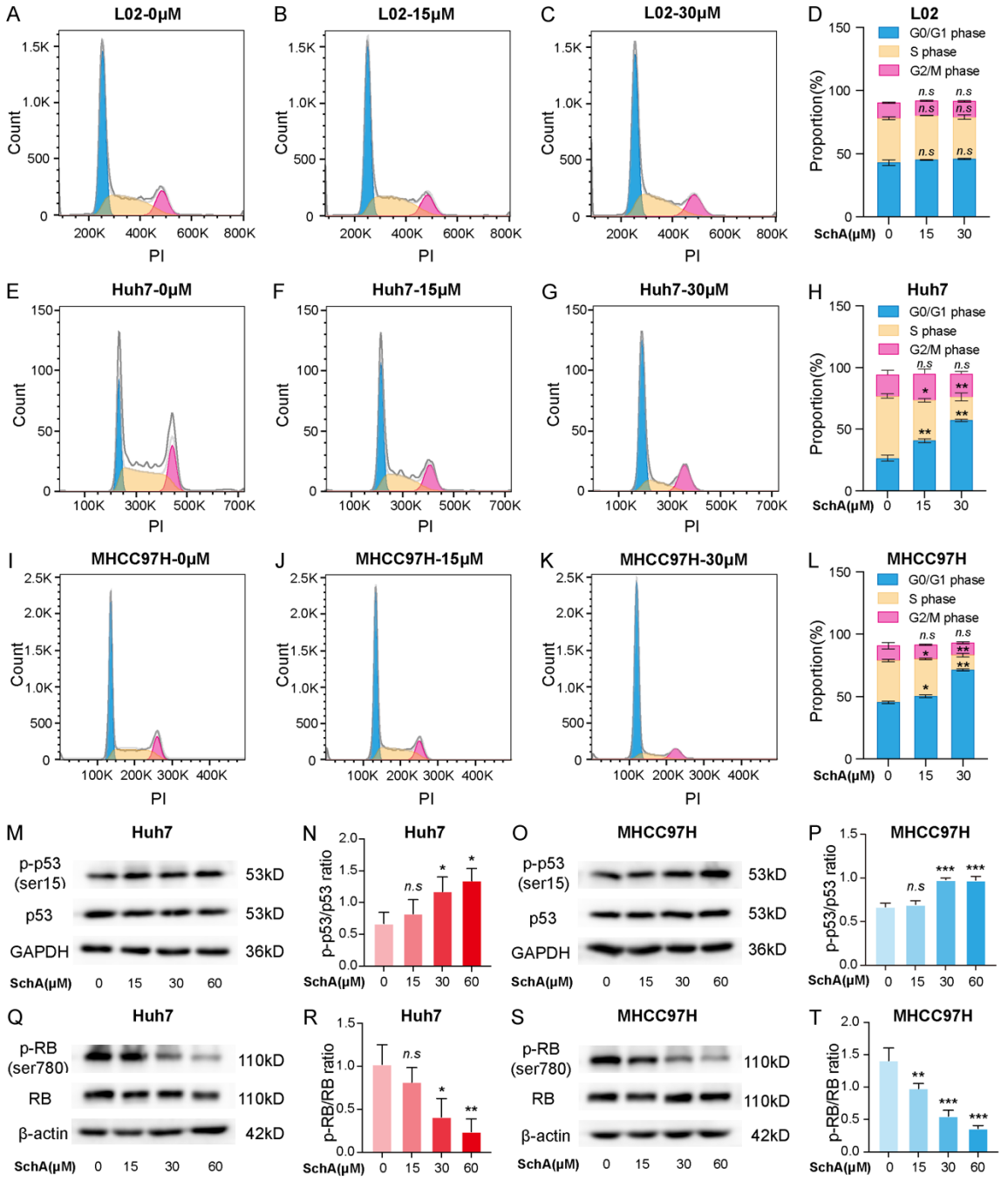

Figure 2. FACS analysis of cell cycle and associated protein expression in SchA treated HCC cells. (A-C) Representative histograms of cell cycle assay of L02 cells treated with different concentration of SchA (0 μM, 15 μM, 30 μM). (D) Statistics of the proportion of different cell cycle phase from (A-C), *n*=3. (E-G) Representative histograms of cell cycle assay of Huh7 cells treated with different concentration of SchA (0 μM, 15 μM, 30 μM). (H) Statistics of the proportion of different cell cycle phase from (E-G), *n*=3. (I-K) Representative histograms of cell cycle assay of MHCC97H cells treated with different concentration of SchA (0 μM, 15 μM, 30 μM). (L) Statistics of the proportion of different cell cycle phase from (I-K), *n*=3. (M) Western blot assessment of p53 and p-p53 in Huh7 cells treated with different concentation of SchA (0 μM, 15 μM, 30 μM, 60 μM). (N) Statistics of p-p53/p53 ratio in (M), *n*=3. (O) Western blot assessment of p53 and p-p53 in MHCC97H cells treated with different concentation of SchA (0 μM, 15 μM, 30 μM, 60 μM). (P) Statistics of p-p53/p53 ratio in (O), *n*=3. (Q) Western blot detection assessment of RB and p-RB in Huh7 cells treated with different concentation of SchA (0 μM, 15 μM, 30 μM, 60 μM). (R) Statistics of p-RB/RB ratio in (Q), *n*=3. (S) Western blot assessment of RB and p-RB in MHCC97H cells treated with different concentation of SchA (0 μM, 15 μM, 30 μM, 60 μM). (T) Statistics of p-RB/RB ratio in (S), *n*=3. One-Way AVONA, **P*<0.05, ***P*<0.01. ****P*<0.001, *n.s* represents no significance.

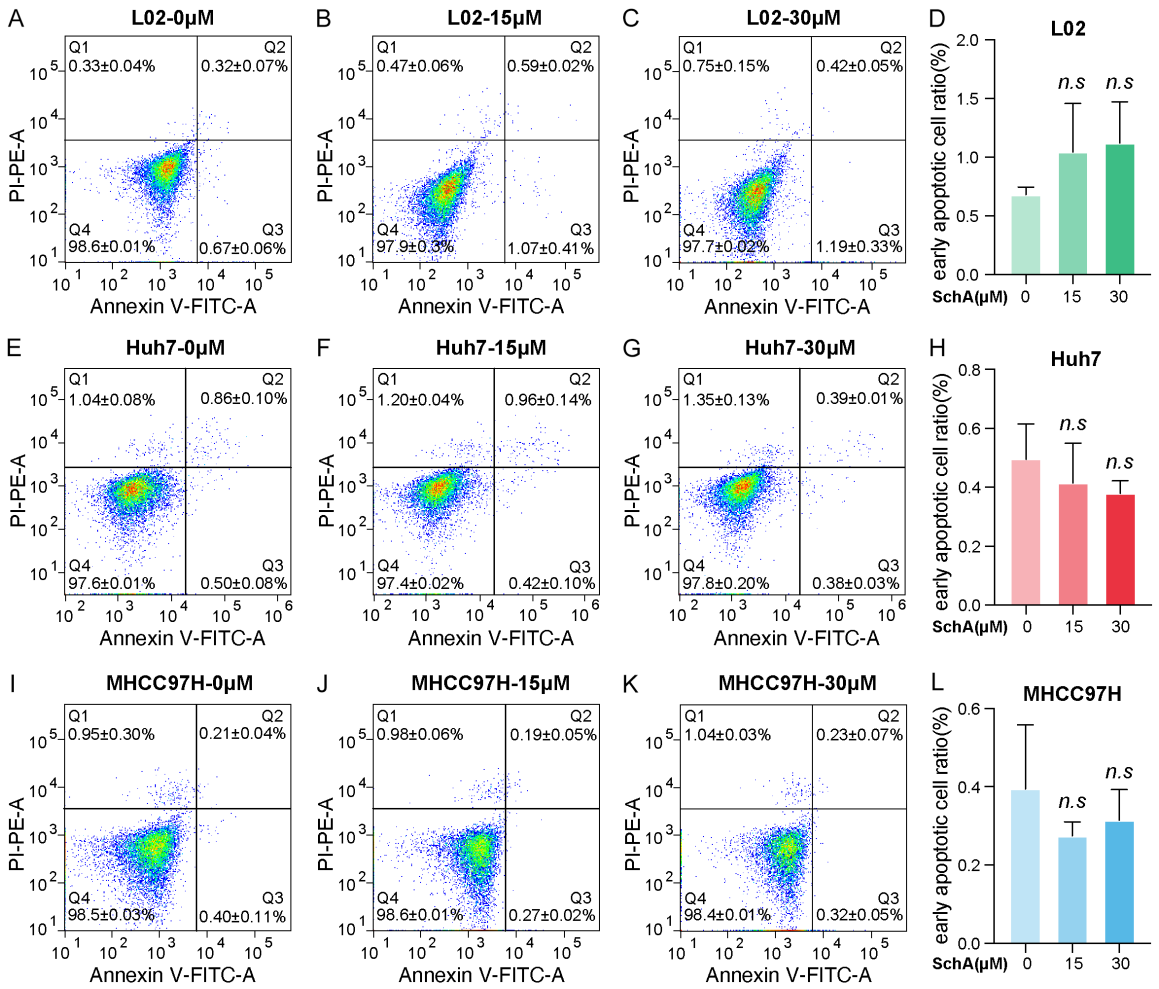

Figure 3. FACS analysis of apoptosis in SchA treated HCC cells. (A-C) FACS plots of L02 cells treated with different concentration of SchA (0 μM, 15 μM, 30 μM) by cell apoptosis assay. (D) Statistics of early apoptotic cell ratio (Q3) from (A-C), *n*=3. (E-G) FACS plots of Huh7 cells treated with different concentration of SchA (0 μM, 15 μM, 30 μM) by cell apoptosis assay. (H) Statistics of early apoptotic cell ratio (Q3) from (E-G), *n*=3. (I-K) FACS plots of MHCC97H cells treated with different concentration of SchA (0 μM, 15 μM, 30 μM) by cell apoptosis assay. (L) Statistics of early apoptotic cell ratio (Q3) from (I-K), *n*=3. Unpaired Student's *t* test, *n.s* represents no significance.

upregulated DEGs from both datasets. As shown in **Figure 4B**, this yielded 464 common upregulated genes. Next, integrating data from TCGA related to liver hepatocellular carcinoma (LIHC), we performed LASSO regression analysis (**Figure 4C**, **4D**) to screen for genes associated with poor prognosis in LIHC, resulting in 21 candidate genes (Supplementary Table 1). We then subjected these 21 genes to further screening using COX regression analysis, ultimately identifying 13 genes highly associated with sorafenib resistance (Supplementary Figure 2). The expression changes of these 13 genes in SchA-treated Huh7 cells were analyzed using a heatmap. As depicted in **Figure 4E**, treatment with SchA induced significant downregulation in over half of these genes in Huh7 cells. Finally, we performed drug sensitivity analysis using the transcriptomic data from SchA treated Huh7 cells (**Figure 4F**). The results demonstrated a significant decrease in the drug sensitivity index following SchA treatment, indicating enhanced sensitivity of HCC cells to sorafenib.

Schisandrin A potentiates sorafenib efficancy in HCC tumor

Based on bioinformatic evidence that SchA increases the sensitivity of HCC cells to sorafenib, we next examined whether SchA could act synergistically with sorafenib to suppress HCC growth. A CCK-8 assay in Huh7 cells

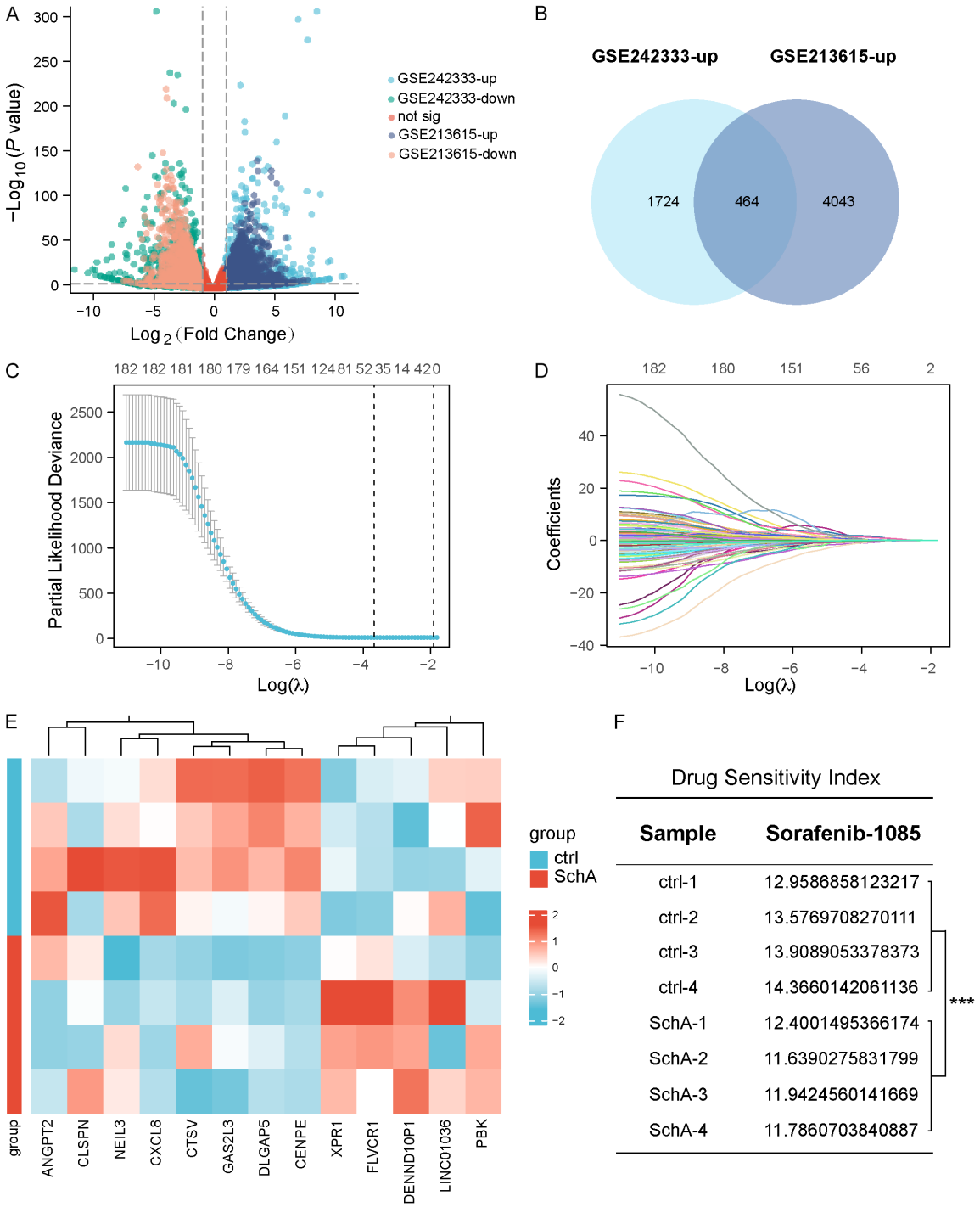

Figure 4. Schisandrin A downregulates sorafenib resistance associatied key genes. (A) Intergrated vocalno plots of DEGs from GSE242333 and GSE213615. (B) Venn diagram showing the intersection of upregulated DEGs in GSE242333 and GSE213615. (C) LASSO regression identifies the prognostic factors out of intersecting genes in (B). (D) Coefficient trajectory plot in LASSO regression. (E) Heatmap of 13 identified genes in transcriptomic data of SchA treated Huh7 cells, compared with control. (F) Transcriptome-based profiling of sorafenib sensitivity in Schisandrin A treated Huh7 cells. Unpaired Student's *t* test, ***P<0.001.

first confirmed a significant synergistic inhibitory effect between SchA and sorafenib (Supplementary Figure 3). Therefore, we established a Huh7 xenograft tumor model in mice (**Figure 5A**). Mice were divided into four treatment groups: control, SchA alone, sorafenib

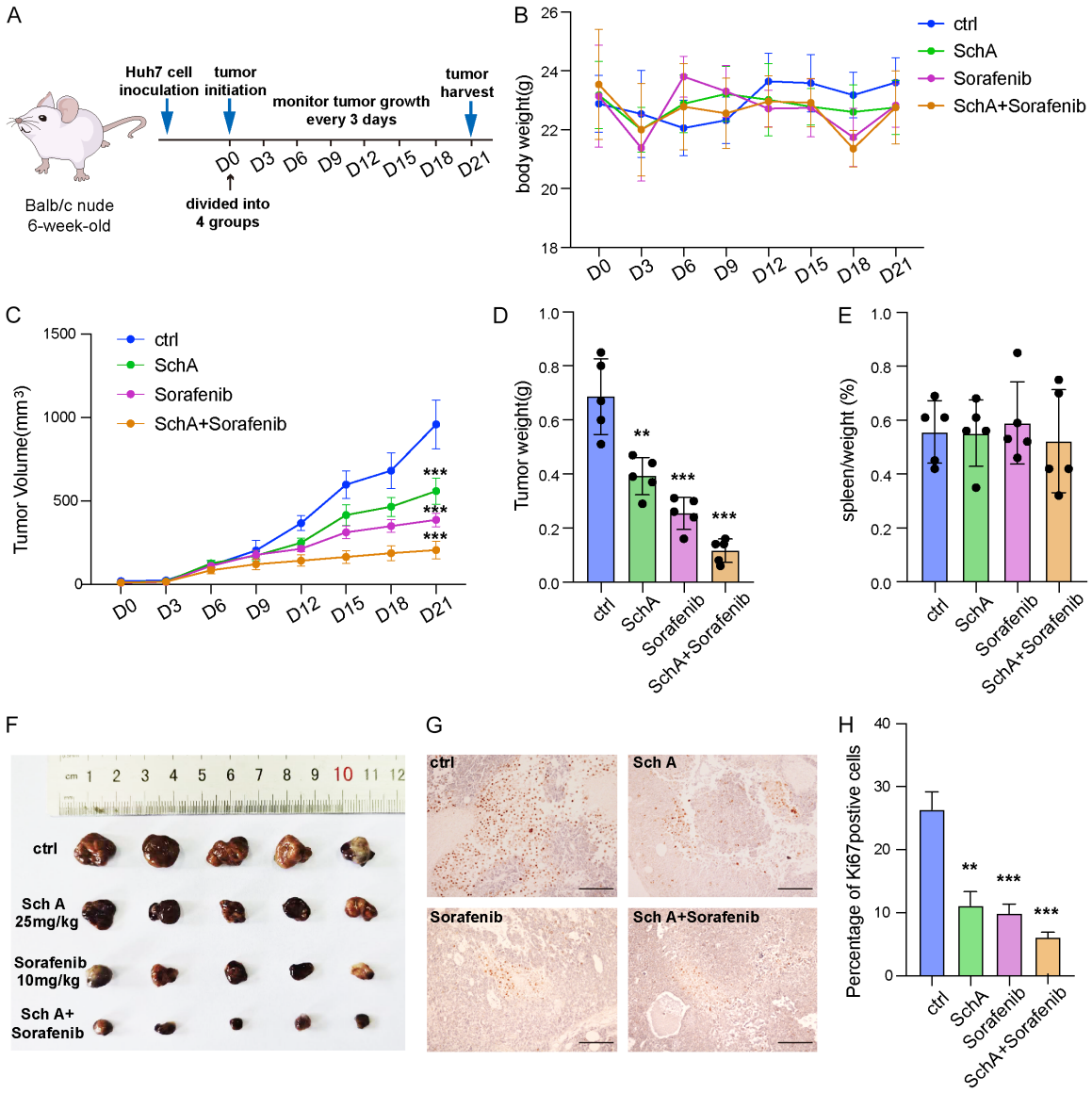

Figure 5. Schisandrin A improves sensitivity of HCC tumor xenograft to sorafenib. (A) Schematic illustration of HCC xenograft mouse model and drug treatment regimen. (B) Longitudinal assessment of body weight in HCC xenograft mouse models during drug treatment, *n*=5. (C) Tumor volume assessment of HCC xenograft mouse models, *n*=5. (D, E) Statistics of tumor weight (D) and spleen/weight ratio (E) at D21, *n*=5. (F) Representative gross morphology of resected HCC Xenografts following Schisandrin A and sorafenib based therapies. (G) Comparative IHC analysis of Ki67 expression in resected HCC xenografts, scale bar: 100 μm, magnification: 200×. (H) Quantification of Ki67 positive cells in (G). One-way repeated measures ANOVA (C), unpaired Student's *t* test (D, E, H), ***P*<0.01, ****P*<0.001.

alone, and SchA + sorafenib combination. Body weight and tumor volume were monitored throughout the treatment period. No significant differences in body weight emerged among the groups (**Figure 5B**). Tumor volumes, however, were significantly smaller in both monotherapy groups than in the control group, and were further reduced in the combination group relative to either treatment alone (**Figure 5C**). At the endpoint, tumors were excised and weighed. Tumor weights were significantly lower in the monotherapy groups than in the control, and the combination group exhibited the lowest tumor weight overall (**Figure 5D**). Notably, spleen index did not differ between four groups (**Figure 5E**). Representative pictures of excised tumor tissues were shown in **Figure 5F**. Staining for Ki67 of tumor tissue sections by immunohistochemistry (**Figure 5G**, **5H**) showed fewer Ki67-positive cells in all groups of mono-

therapy than in control group, and there was the largest difference in the combination group, which exhibited the weakest cell proliferation. All these data indicate that Schisandrin A synergistically augments the anti-tumor effect of sorafenib on HCC.

Multi-omics analysis of the mechanism of SchA

To identify the effects of SchA on downstream genes expressed and signalling pathways in HCC cells, we analysed RNA sequencing (RNA-seq) data from control (Ctrl) and SchA-treated Huh7 and MHCC97H cells. DEGs (differentially expressed genes) induced by SchA treatment were identified. The results showed that SchA induced huge changes in gene expression in the two cell lines. For Huh7 cells (**Figure 6A**), 228 DEGs were identified, 144 DEGs were upregulated genes and 84 DEGs were downregulated genes. For MHCC97H cells (**Figure 6B**), 157 DEGs were identified, 36 DEGs were upregulated genes and 121 DEGs were downregulated genes. We then analysed Gene Ontology (GO) and Kyoto Encyclopedia of Genes and Genomes (KEGG) pathways enrichment of DEGs from Huh7 cells and MHCC97H cells. Both analyses revealed that the DEGs generated by SchA treatment in Huh7 and MHCC97H cells were mainly enriched in processes related to liver functions, such as cholesterol biosynthesis and metabolism (**Figure 6C**, **6D**). Because the transcriptomic analysis indicated that SchA might regulate the metabolic switch of HCC cells, we then analysed the cell samples by an untargeted metabolomics method. A joint pathway analysis was then conducted on both transcriptomics data and metabolomics data to further discover the metabolism-associated signalling pathways generated by SchA. Our analysis showed that SchA treatment dramatically decreased the retinol metabolism pathway in both Huh7 and MHCC97H cells (**Figure 6E**, **6F**), which provides a necessary basis for subsequent study of the mechanism.

Discussion

Advanced HCC is extremely hard to cure due to its few treatment options. For patients with unresectable HCC, the primary treatment is targeted systemic treatment. Sorafenib, the first multiple kinase inhibitor approved by the FDA for advanced HCC, extends survival time of advanced HCC by inhibiting tumor angiogenesis and cell proliferation. However, the clinical effect of sorafenib is not sustained. Drug resistance usually occurs within 4 to 5 months of continuous drug administration, so the efficacy of sorafenib is greatly restricted in the long term. Due to the quick loss of the therapeutic effect, more strategies to avoid acquired drug resistance and restore the tumor sensitivity by combination treatment are developed to better improve patient outcomes [21].

Traditional Chinese Medicine formulations have strong therapeutic relevance for cancer treatment [22]. For example, icaritin, a natural compound isolated from the herb *Epimedium*, has been approved by Chinese Medicines Administration for advanced and inoperable HCC. This agent lowers the mortality risk by inhibiting the growth of tumor and regulating the immune response [23, 24]. Postoperative application of HuaChanSu and Huaier granule can obviously improve liver function and quality of life of patients with HCC [25, 26]. Of note, these granules can enhance antitumor effect of sorafenib in HCC [27, 28]. Together, these results showed the potential of natural agents to serve as an adjuvant of conventional targeted therapies [22]. Based on this background, we focused on Schisandrin A, one of the active ingredients in *Schisandra chinensis*, and showed its strong antitumor effect against HCC and their sensitivity-inducing capacity to malignant cells for sorafenib. These results provide new potential clinical directions for incorporating traditional medicine into modern HCC treatments.

Schisandra chinensis is a traditional medicinal herb for traditional Chinese medicine and it has proven hepatoprotective, cardioprotective and immunomodulatory effects. The major bioactive components of Schisandra are the Schisandra lignans [9]. Schisandrin A, also named Deoxyschizandrin, is a major lignan component of the Schisandra herb, with substantial attention to its antitumor effect, especially on HCC. A previous study found that Schisandrin A triggers ferroptosis in HCC cells by increasing mitochondrial reactive oxygen species (ROS), activating the AMPK pathway and inactivation mTOR pathway [29]. Our study was to investigate the direct antitumor effects of Schisandrin A and investigate its practical value in combination treatment. We first evaluated the activities of this drug using classic *in*

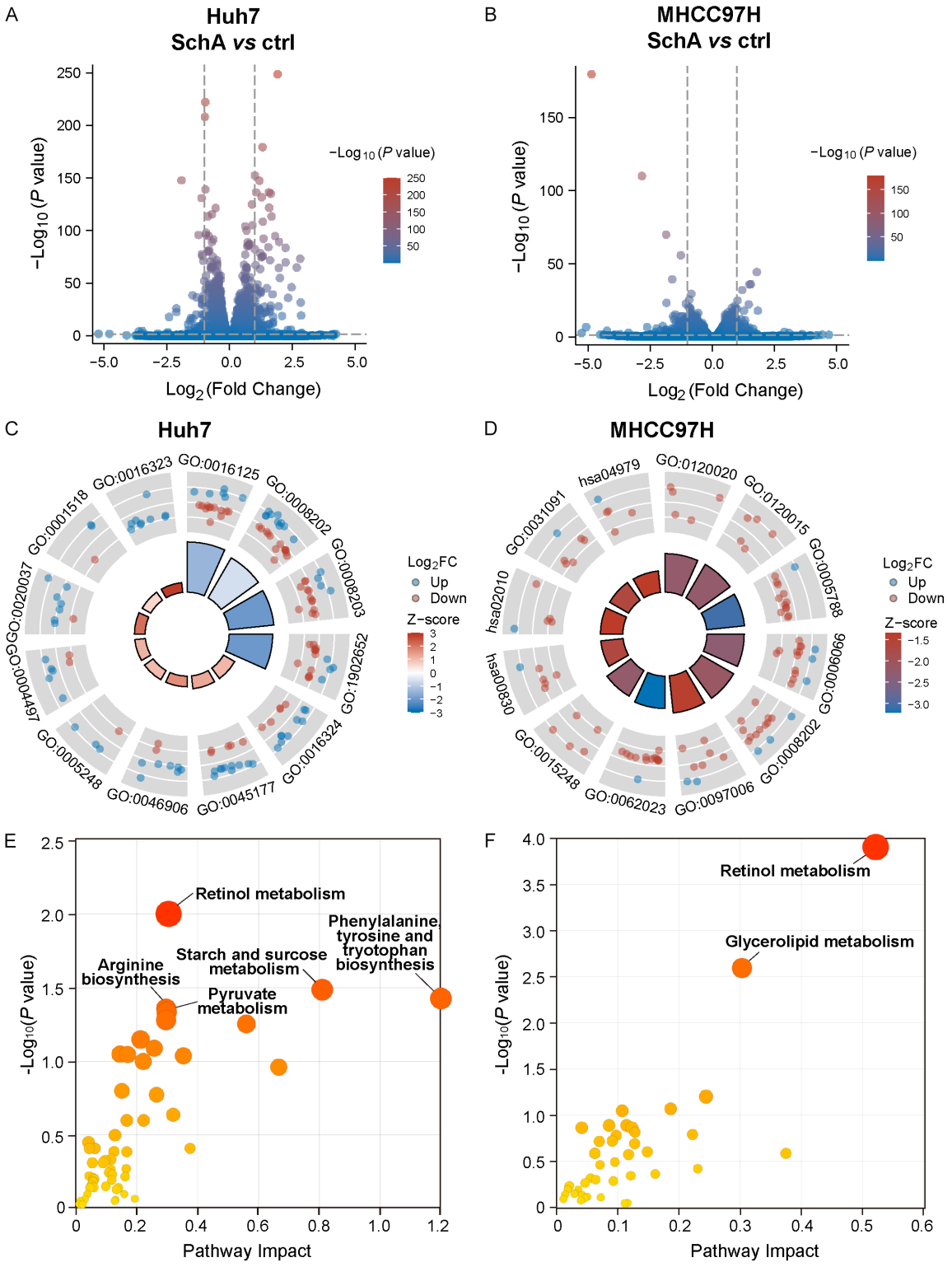

Figure 6. Bioinformatical analysis of HCC cells treated with SchA. (A) Vocalno plots showing DEGs in SchA treated Huh7 cells compared with control, cutoff: $|\log_2(\text{Fold Change})|>1$, adjusted *P* value <0.05. (B) Vocalno plots showing DEGs in SchA treated MHCC97H cells compared with control, cutoff: $|\log_2(\text{Fold Change})|>1$, adjusted *P* value <0.05. (C) Combined GO and KEGG analysis of DEGs in (A). (D) Combined GO and KEGG analysis of DEGs in (B). (E) Joint pathway analysis integrating transcriptomic and metabolomic profiles in SchA-treated Huh7 cells. (F) Joint pathway analysis integrating transcriptomic and metabolomic profiles in SchA-treated MHCC97H cells.

vitro and *in vivo* studies. Furthermore, our data showed that Schisandrin A can induce cell cycle arrest of HCC cells, markedly inhibits cell proliferation of HCC cells and markedly inhibits tumor growth *in vivo*.

With this information in hand, we were interested in the clinical impact of these findings. We therefore investigated whether Schisandrin A could synergistically enhance the effects of sorafenib, a first-line targeted drug therapy for HCC. A key problem of sorafenib therapy is the frequent occurrence of acquired treatment resistance. To address this problem, we analyzed transcriptome data from sorafenib-resistant HCC cell lines and then used the data together with survival data from patients to look for key genes related to treatment resistance. We then used computational modeling to predict whether the pharmacological effects of Schisandrin A that are known to us can affect those resistance-related genes and result in recovery of sorafenib sensitivity. The computational modelling suggested that Schisandrin A could in fact reverse the resistant phenotype. To confirm this prediction, we evaluated the combination of Schisandrin A and sorafenib in cell culture and in animal tumor models. Our results demonstrated that co-administration of Schisandrin A greatly increased the cytotoxic effect of sorafenib against HCC cells.

For full understanding of the molecular mechanisms mediating the antitumor and sorafenib-sensitizing effects of Schisandrin A, we employed transcriptomic and metabolomic profiling. Our study revealed the pharmacological efficacy of Schisandrin A with respect to modulation of retinol metabolism. Previously, the retinol metabolic pathway was reported to be hyperactivated during HCC progression [30]. In terms of drug response, excessive retinoic acid, one of the core downstream metabolites of retinol, leads to acquired sorafenib resistance mainly via providing resistance to ferroptosis. Inhibition of this metabolic pathway effectively reversed resistance and resensitized HCC cells to sorafenib [31]. Connecting the above observations with our multi-omics results, we proposed that Schisandrin A could mediate the abrogation of aberrantly activated retinol metabolism, thus directly inhibiting the progression of HCC and simultaneously erasing metabolic protection from sorafenib, which accounts for the synergistic therapeutic effect.

In summary, we showed that Schisandrin A inhibits HCC cell proliferation by inducing cell cycle arrest and significantly sensitizes malignant cells to sorafenib. Although its molecular targets are not completely clear, integration of data from multiple biological datasets leads us to conclude that Schisandrin A leads to synergistic effect by inhibiting hyperactivated retinol metabolism. These data indicate the therapeutic value of Schisandrin A used as supplementary therapy with standard targeting therapy and provide experimental evidences for its use in clinical trials in patients with hepatocellular carcinoma.

Acknowledgements

The authors gratefully acknowledge the support for this research provided by the Startup Fund of Hubei Shizhen Laboratory. National Natural Science Foundation of China (Grant No. 82405575), Natural Science Foundation of Hubei Province (Grant No. 2024AFD318, No. 2024AFD305), General Program of China Postdoctoral Science Foundation (Grant No. 2024-M750854, No. 2023M74110), Postdoctoral Fellowship Program of CPSF (Grant No. CZC20240445), Natural Science Foundation of Wuhan (Chenguang Program, Grant No. 2024040801020334), Scientific Research Plan of the Hubei Provincial Department of Education (No. Q20232009), Health and Health Technology Project of Hubei Provincial (WJ2025Q041).

Disclosure of conflict of interest

None.

Address correspondence to: Shuai Zha, School of Laboratory Medicine, Hubei University of Chinese Medicine, No. 16 Huangjiahu West Road, Hongshan District, Wuhan 430065, Hubei, PR China. E-mail: shuaizha1@hbucm.edu.cn; Deliang Zhou, Department of General Surgery, Affiliated Hospital of Hubei University of Chinese Medicine, Hubei Provincial Hospital of Traditional Chinese Medicine, Hubei Province Academy of Traditional Chinese Medicine, No. 4 Huayuanshan, Wuchang District, Wuhan 430060, Hubei, PR China. E-mail: zdl_hbucm@163.com

References

[1] Moris D, Martinino A, Schiltz S, Allen PJ, Barbas A, Sudan D, King L, Berg C, Kim C, Bashir

M, Palta M, Morse MA and Lidsky ME. Advances in the treatment of hepatocellular carcinoma: an overview of the current and evolving therapeutic landscape for clinicians. CA Cancer J Clin 2025; 75: 498-527.

[2] Gao W, Pan ZL, Zhao XH, Yang L, Cao JB, Li DY, Zheng HJ, Liu C, Li GT, Bao X, Liu XM, Zhang WH, Zhu XL, Xiao BH, Song TQ, Li Q, Lu W, Xing WG and Zhang W. Donafenib and sintilimab combined with hepatic arterial infusion chemotherapy for unresectable hepatocellular carcinoma: a prospective, single-arm phase II trial (DoHAICs study). EClinicalMedicine 2025; 83: 103217.

[3] Llovet JM, Ricci S, Mazzaferro V, Hilgard P, Gane E, Blanc JF, de Oliveira AC, Santoro A, Raoul JL, Forner A, Schwartz M, Porta C, Zeuzem S, Bolondi L, Greten TF, Galle PR, Seitz JF, Borbath I, Haussinger D, Giannaris T, Shan M, Moscovici M, Voliotis D and Bruix J; SHARP Investigators Study Group. Sorafenib in advanced hepatocellular carcinoma. N Engl J Med 2008; 359: 378-390.

[4] Dong X, Zhang T, Zhang C, Shang W, Zhang Y and Zhang X. Traditional Chinese herbal medicines for the treatment of ischemic stroke in China. Ageing Res Rev 2025; 110: 102803.

[5] Li J, Zhang H, Ruan H, Zhao G, He H, Hou C, Sun W, Hou S, Liu X and Li Y. Efficacy and safety of Chinese medicine in treating risk window of AECOPD: a multicenter randomized controlled trial. Phytomedicine 2025; 144: 156903.

[6] Li S, Chen X, Shi H, Yi M, Xiong B and Li T. Tailoring traditional Chinese medicine in cancer therapy. Mol Cancer 2025; 24: 27.

[7] Yang Y, Ge W, Luo W, Yang Y, Duo H, Kuang X, Xiao H, Jiang H, Xiong K, Zhao H and Yang X. Effects of Chinese herbal medicine on the secondary prevention of chemotherapy-induced thrombocytopenia in malignant solid tumors, a randomized clinical trial. Phytomedicine 2025; 144: 156871.

[8] Cui D, Zhang C, Zhang L, Zheng J, Wang J, He L, Jin H, Kang Q, Zhang Y, Li N, Sun Z, Zheng W, Wei J, Zhang S, Feng Y, Tan W and Zhong Z. Natural anti-cancer products: insights from herbal medicine. Chin Med 2025; 20: 82.

[9] He D, Pei X, Liu B, Li J, Dong J, Efferth T and Ma P. Lignan contents of Schisandra chinensis (Turcz.) Baill. from different origins-A new model for evaluating the content of prominent components of Chinese herbs. Phytomedicine 2024; 128: 155361.

[10] Xu H, Sun L, Du Y, Duan W, Li W, Luo S, Liang B, Ma C and Pan G. Magnetic molecularly imprinted polymer combined with solid-phase extraction for purification of schisandra chinensis lignans. Polymers (Basel) 2024; 16: 3124.

[11] Liu HL, Huang Z, Li QZ, Cao YZ, Wang HY, Alolgab RN, Deng XY and Zhang ZH. Schisandrin A alleviates renal fibrosis by inhibiting PKCbeta and oxidative stress. Phytomedicine 2024; 126: 155372.

[12] Zeng J, Liao S, Liang Z, Li C, Luo Y, Wang K, Zhang D, Lan L, Hu S, Li W, Lin R, Jie Z, Hu Y, Dai S and Zhang Z. Schisandrin A regulates the Nrf2 signaling pathway and inhibits NLRP3 inflammasome activation to interfere with pyroptosis in a mouse model of COPD. Eur J Med Res 2023; 28: 217.

[13] Li B, Zhou W, Zhang J, Wang N, Yang X and Ge X. Schisandrin a ameliorates cardiac injury and dysfunction induced by hemorrhagic shock via activating the Nrf2 signaling pathway. Am J Chin Med 2024; 52: 2453-2468.

[14] Jin J, Chen M, Wang H, Li S, Ma L and Wang B. Schizandrin A attenuates early brain injury following subarachnoid hemorrhage through suppressing neuroinflammation. Mol Biol Rep 2024; 51: 236.

[15] Guo X, Lei M, Ma G, Ouyang C, Yang X, Liu C, Chen Q and Liu X. Schisandrin A alleviates spatial learning and memory impairment in diabetic rats by inhibiting inflammatory response and through modulation of the PI3K/AKT pathway. Mol Neurobiol 2024; 61: 2514-2529.

[16] Zhu L, Wang Y, Lv W, Wu X, Sheng H, He C and Hu J. Schizandrin A can inhibit non-small cell lung cancer cell proliferation by inducing cell cycle arrest, apoptosis and autophagy. Int J Mol Med 2021; 48: 214.

[17] Zhu L, Wang Y, Huang X, Liu X, Ye B, He Y, Yu H, Lv W, Wang L and Hu J. Schizandrin A induces non-small cell lung cancer apoptosis by suppressing the epidermal growth factor receptor activation. Cancer Med 2024; 13: e6942.

[18] Peng CW, Ma PL and Dai HT. Schizandrin A promotes apoptosis in prostate cancer by inducing ROS-mediated endoplasmic reticulum stress and JNK MAPK signaling activation. Pathol Res Pract 2025; 269: 155889.

[19] Chen BC, Tu SL, Zheng BA, Dong QJ, Wan ZA and Dai QQ. Schizandrin A exhibits potent anticancer activity in colorectal cancer cells by inhibiting heat shock factor 1. Biosci Rep 2020; 40: BSR20200203.

[20] Chi B, Sun Y, Zhao J and Guo Y. Deoxyschizandrin inhibits the proliferation, migration, and invasion of bladder cancer cells through ALOX5 regulating PI3K-AKT signaling pathway. J Immunol Res 2022; 2022: 3079823.

[21] Li Y, Yang W, Zheng Y, Dai W, Ji J, Wu L, Cheng Z, Zhang J, Li J, Xu X, Wu J, Yang M, Feng J and Guo C. Targeting fatty acid synthase modulates sensitivity of hepatocellular carcinoma

to sorafenib via ferroptosis. J Exp Clin Cancer Res 2023; 42: 6.
[22] Man S, Luo C, Yan M, Zhao G, Ma L and Gao W. Treatment for liver cancer: from sorafenib to natural products. Eur J Med Chem 2021; 224: 113690.
[23] Wei W, Wang H, Fu L and Liu H. Icaritin induces paraptosis in hepatocellular carcinoma cells by targeting BHLHE40 via endoplasmic reticulum stress and mitochondrial dysfunction. Phytomedicine 2025; 143: 156870.
[24] Qin SK, Li Q, Ming Xu J, Liang J, Cheng Y, Fan Y, Jiang J, Ye H, Tao H, Li L, Zheng L, Wei Z, Li S, Meng K, Ye B and Sun Y. Icaritin-induced immunomodulatory efficacy in advanced hepatitis B virus-related hepatocellular carcinoma: immunodynamic biomarkers and overall survival. Cancer Sci 2020; 111: 4218-4231.
[25] Wu Q, Chen Q, Yang J, Zhang J and Yang A. Material basis revelation of anti-hepatoma effect of Huachansu (Cinobufacini) through down-regulation of thymidylate synthase. Chin Herb Med 2024; 17: 127-138.
[26] Wu J, Tang G, Cheng CS, Yeerken R, Chan YT, Fu Z, Zheng YC, Feng Y and Wang N. Traditional Chinese medicine for the treatment of cancers of hepatobiliary system: from clinical evidence to drug discovery. Mol Cancer 2024; 23: 218.
[27] Jiang HY, Zheng HM, Xia C, Li X, Wang G, Zhao T, Cui XN, Wang RY and Liu Y. The research progress of Bufalin in the treatment of hepatocellular carcinoma. Onco Targets Ther 2022; 15: 291-298.
[28] Zhang Z, Shen C and Zhou F. The natural medicinal fungus Huaier promotes the anti-hepatoma efficacy of sorafenib through the mammalian target of rapamycin-mediated autophagic cell death. Med Oncol 2022; 39: 221.
[29] He LW, Lin CJ, Zhuang LJ, Sun YH, Li YC and Ye ZY. Targeting hepatocellular carcinoma: Schisandrin A triggers mitochondrial disruption and ferroptosis. Chem Biol Drug Des 2024; 104: e70010.
[30] Jeong JM, Choi SE, Shim YR, Kim HH, Lee YS, Yang K, Kim K, Kim MJ, Chung KPS, Kim SH, Byun JS, Eun HS and Jeong WI. CX3CR1^{+} macrophages interact with HSCs to promote HCC through CD8+ T-cell suppression. Hepatology 2025; 82: 655-668.
[31] Tian Y, Bao X, Lei S, Huang Y, Wang X, Tu Y, He Q, Zhang F, Xu H, Ashrafizadeh M, Sethi G, Wang F and Zeng Z. *In vivo* CRISPR screening identifies POU3F3 as a novel regulator of ferroptosis resistance in hepatocellular carcinoma via retinoic acid signaling. Cell Commun Signal 2025; 23: 329.

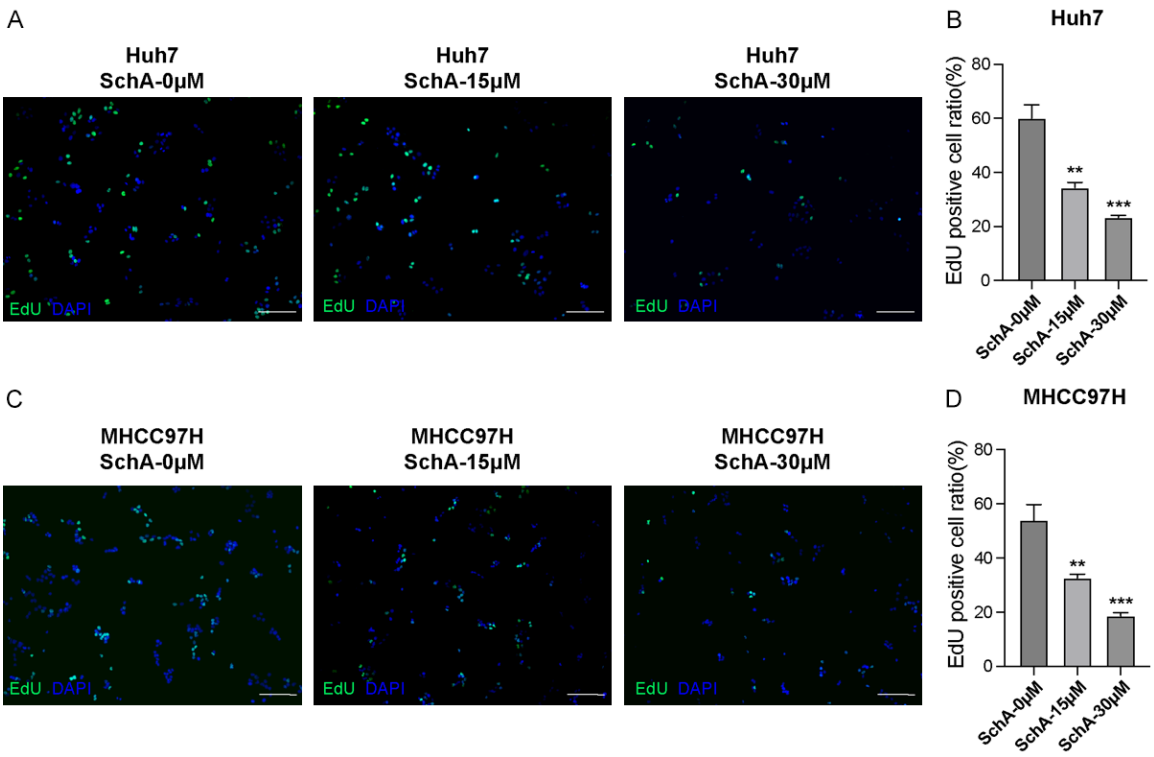

Supplementary Figure 1. EdU incorporation of SchA treated HCC cells.

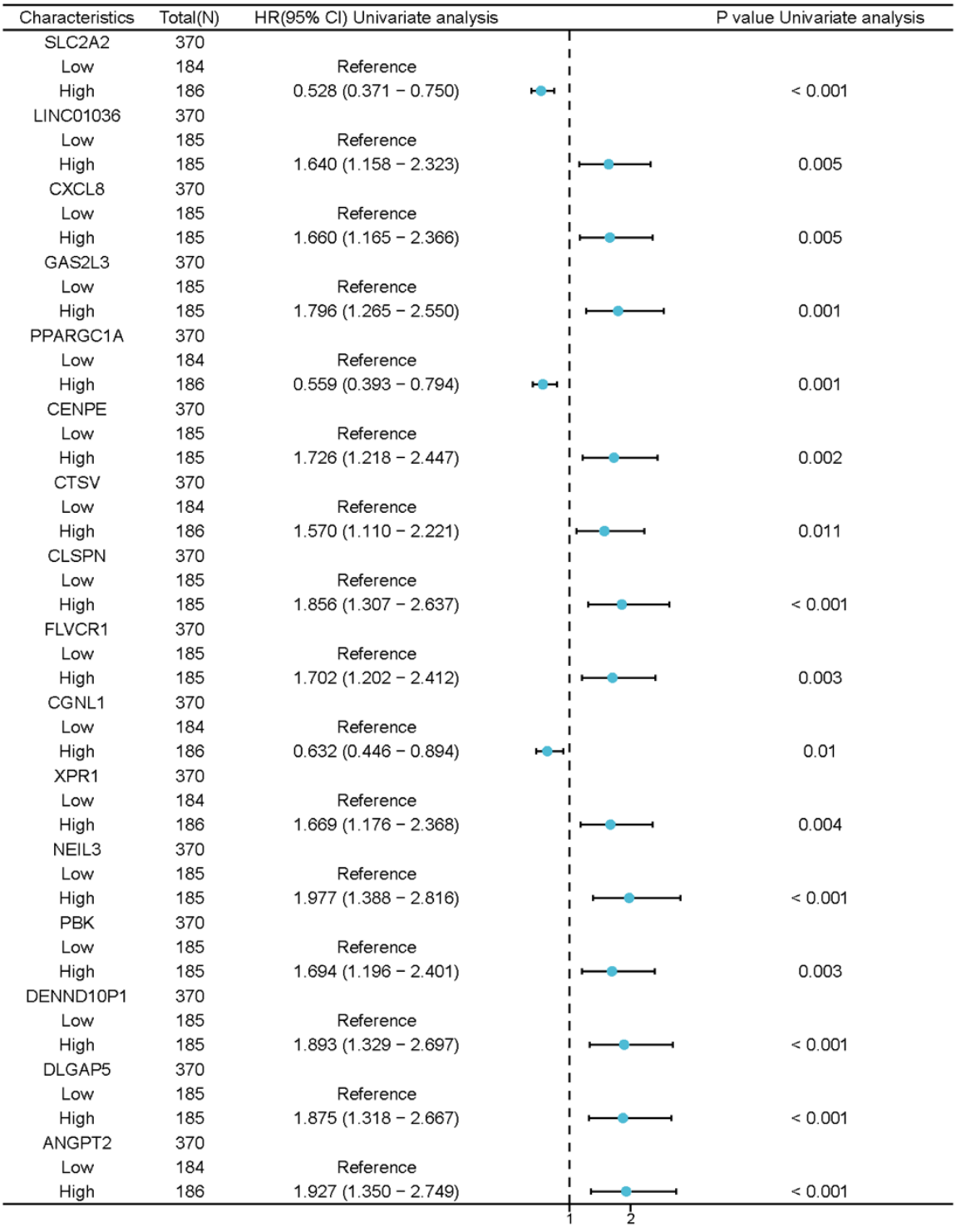

Supplementary Figure 2. COX regression of identified genes.

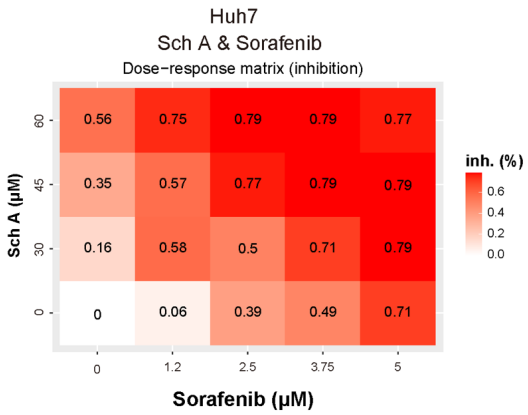

Supplementary Figure 3. The synergistic effect of SchA and Sorafenib on Huh7 cells.